

<sup>1</sup> PREPARED FOR SUBMISSION TO JINST

<sup>2</sup> **Directional Xenon Measurement**

---

<sup>3</sup> ABSTRACT: Abstract...

<sup>4</sup> KEYWORDS: Only keywords from JINST's keywords list please

<sup>5</sup> ARXIV EPRINT: [1234.56789](https://arxiv.org/abs/1234.56789)

---

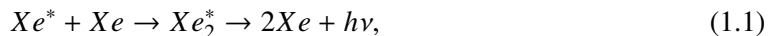
<b>6</b>	<b>Contents</b>		
<b>7</b>	<b>1</b>	<b>Introduction</b>	<b>1</b>
<b>8</b>	<b>2</b>	<b>Experimental Setup</b>	<b>2</b>
9	2.1	Gas handling system	2
10	2.2	The Cryogenic system	3
11	2.3	The Detector	5
12	2.3.1	The Detector Chamber	5
13	2.3.2	The Sphere	6
<b>14</b>	<b>3</b>	<b>The Data Acquisition (DAQ) System</b>	<b>8</b>
<b>15</b>	<b>4</b>	<b>Simulation</b>	<b>11</b>
16	4.1	The Detector Geometry	11
17	4.2	The statistical test	11
<b>18</b>	<b>5</b>	<b>Summary</b>	<b>11</b>

---

## **19 1 Introduction**

**20** The use of Noble-liquid detectors in the field of astroparticle physics has increased in the past  
**21** decades. Detectors aiming at measuring Dark Matter (DM) particles and neutrinos properties use  
**22** large liquid argon or liquid xenon (LXe) chambers [1, 2]. Current and future experiment for DM  
**23** detectioin are tuned to detect weakly interacting massive particles (WIMPs), a postulated candiadte  
**24** for DM particle [3]. LXe based detectors are to date the leading in sensitivity and size for these  
**25** searches [4–7].

**26** When a particle interacts within the LXe media, it forms a cloud of excited and ionized states  
**27** with typical length of 100 nm. The excited Xe ( $Xe^*$ ) combines with other Xe atoms to form an  
**28** excited dimer state (excimer) when they decay to ground state they emit light.



**29** The electrons emitted from the ionization can recombine with a surrounding atom, this process of  
**30** recombination provides another possibility to produce excimers,



31 Once  $Xe^*$  is produced it adds to the scintillation process explained in 1.1. There are two types of  
32  $Xe_2^*$  excimer states, singlet and triplet, with lifetime of  $\sim 3$  ns and  $\sim 25$  ns respectively. The wave-  
33 length emitted by these states is between (175-180) nm which is lower than the lowest excitation of  
34 xenon, and therefore travel through it to reach a photo-detector situated outside the LXe. Although  
35 much is measured on these scintillation processes, the basic knowledge of the quantum properties  
36 of these interactions is based on experiments preformed several decades ago.

37 The phenomenon of superradiance in which identical quantum states "communicate" through  
38 electromagnetic field if in close proximity, is well studied. In certain conditions the emission of  
39 photons from these correlated states is very different than the sum of random states. This difference  
40 is in spectral, temporal and spatial properties [8, 9]. Early studies show that scintillation in LXe can  
41 produce coherent amplification of light [10, 11]. These studies were focusing on the macroscopic  
42 ionization using high energy density electron beams.

43 The understanding and quantification of the microscopic effects of non linear phenomena such  
44 as superradiance in Lxe for a single interaction, can improve DM experiments to reduce back-  
45 ground by the extra knowledge of directionality. irreducible background such as coherent neutrino  
46 nucleus scattering of neutrinos from the sun can be discard.

47 In this paper we present an experimental set-up called DIREXENO (Directional Xenon) aim-  
48 ing at measuring the spatial distribution of LXe scintillation light, and quantify non-isotropic emis-  
49 sion.

## 50 2 Experimental Setup

51 The experimental setup that is described in this section, is designed to measure, the spatial and  
52 temporal properties of LXe scintillation. However it is designed in a modular way, so it can serve  
53 different requirements from different future experiments.

54 There are four main building blocks constructing the full setup, a schematics of them with  
55 the interfaces connecting them is shown in Fig. ???. The gas handling system, which, in normal  
56 working mode, drives the xenon from the detector trough a purifier and back into the detector.  
57 The cryogenic system, which liquefies the xenon and delivers it to the detector part. The detector  
58 system, mainly an HPFS sphere with a small bubble of LXe inside it surrounded with PMTs. Finally  
59 the data acquisition (DAQ) system that supplies HV and reads the data from all sensors (e.g., PMTs,  
60 pressure gauge etc.). Each building block can be replaced without effecting the others.

61 The full assembly (Fig. 1) is held on three separate racks, one for the DAQ, while the two  
62 others hold the cryogenic detector and gas handling system are joined using a 100mm bar with  
63 shock absorbers on both sides. Some of the guidelines for the design of DIREXENO are based  
64 on [12]

### 65 2.1 Gas handling system

66 A typical LXe detector must keep a high level of purity. Careful selection and meticulously clean-  
67 ing of all parts before mounting, is needed, however is not sufficient. The desired level of most  
68 detectors of impurity concentration is at the level of 1 ppb  $O_2$  equivalent [1]. This is crucial to  
69 allow ionization electrons drift for several cm. To reach that level in a reasonable amount of time

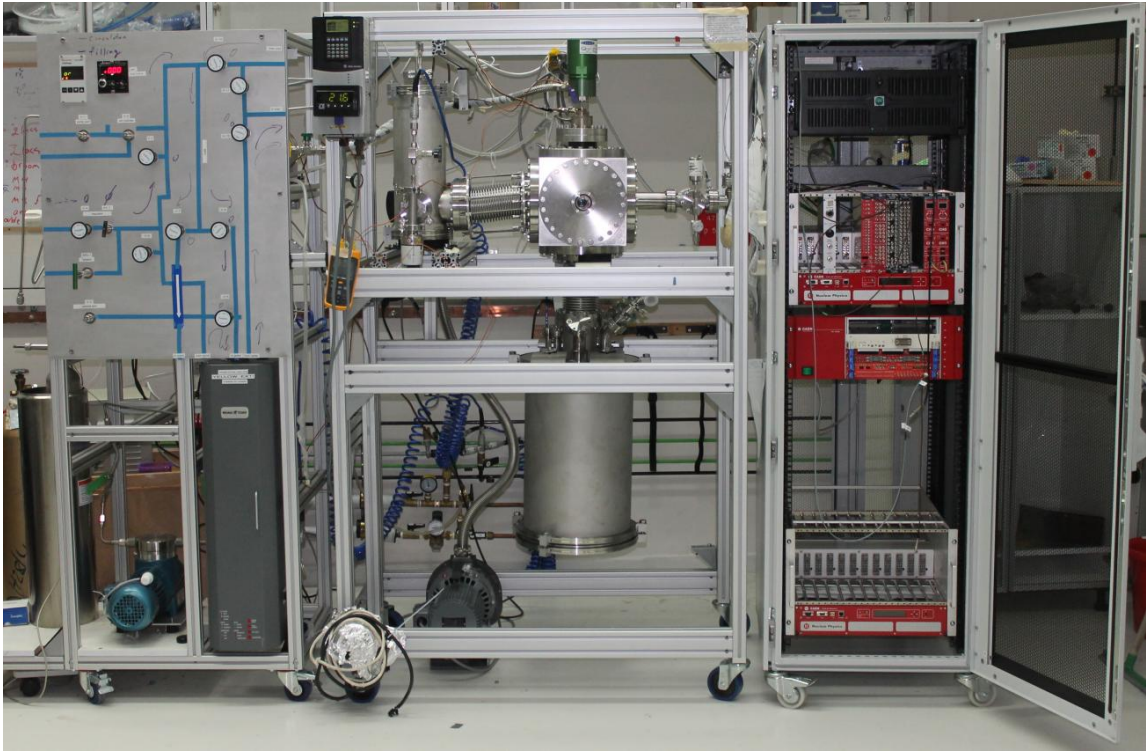


**Figure 1.** DIREXENO. On the left the purification system, in the middle the cryogenic and detector chamber, and on the right the Data acquisition system.

70 (several days instead of months), continuous purification is needed. The gas handling system,  
71 provides this process, alongside with all gas handling operations such as filling and recuperation.

72 During purification mode, xenon is taken from the chamber (in liquid phase) passes through a  
73 heat exchanger<sup>1</sup> where it is heated and vaporized. The xenon is forced by a KNF diaphragm pump  
74 into a hot getter<sup>2</sup> which cleans the xenon from most impurities. The xenon also passes through an  
75 MKS Mass Flow Controller<sup>3</sup> (MFC), this allows monitoring and controlling the amount of xenon  
76 in the system.

77 After the xenon is purified, it is delivered back to the cryogenic system through the heat ex-  
78 changer, there the remained xenon gas is liquefied before it continues back to the chamber. A  
79 schematic of this system is shown in fig. 2.

## 80 2.2 The Cryogenic system

81 Remote cooling is generally used in DM experiments due to background radiating from the cooler  
82 to the detector. Although in our system this is not of great importance there are still several ad-  
83 vantages to remote cooling such as: lowering acoustic noise from the cryo-cooler and flexibility to  
84 design changes. The cryogenic system is connected on one side to the gas system and on the other

<sup>1</sup>GEA GBS100M-24 plate heat exchanger

<sup>2</sup>MONO-TORR PS4-MT15-R-2

<sup>3</sup>MKS mass flow controller

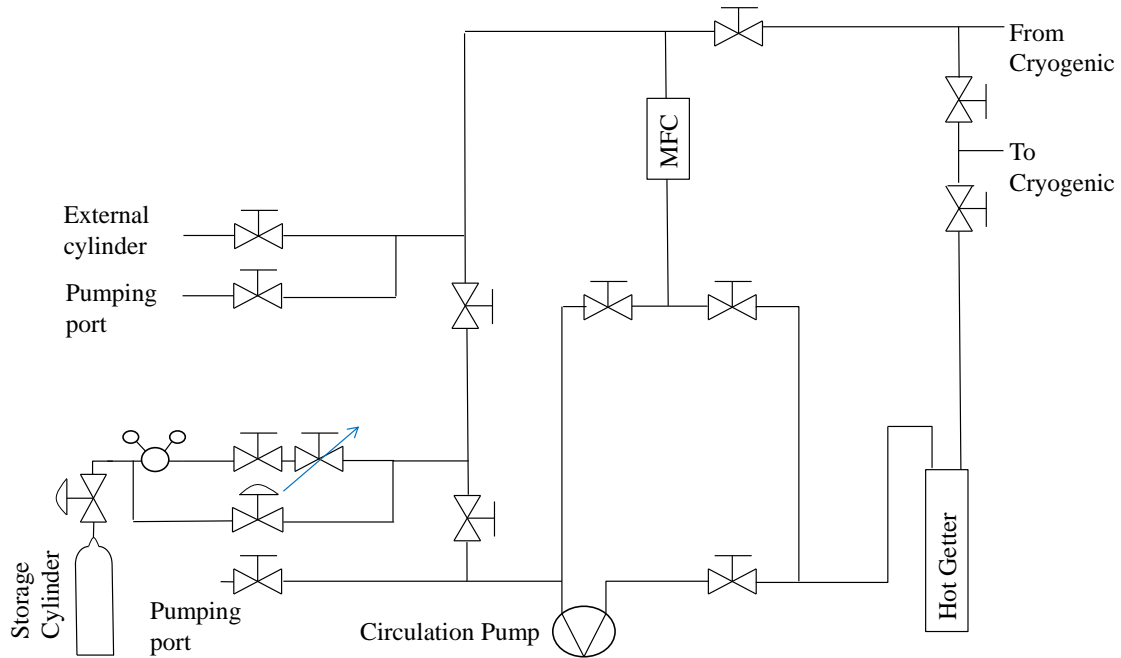


**Figure 2.** Schematics of the purification system. High pressure valves are indicated as valves with arcs. Needle valves are indicated as a valve with an arrow.

85 to the detector chamber, any change in the system (e.g., cooler type or model) requires the change  
 86 of that specific part without changing the detector nor the gas system.

87 The system is made out of two chambers, the outer vessel (OV) which holds the insulation  
 88 vacuum, and the inner vessel (IV) that holds the xenon. In addition to the vacuum which prevents  
 89 heat leaks from diffusion and convection, the entire IV is covered by multi layer aluminized Mylar  
 90 to prevent heating via radiation an image of the detector and the CAD design are shown in Fig 3.

91 The OV is made of a 10" CF cube, with ports on all six faces (e.g., FT, pumping ports, view  
 92 ports). This vacuum is shared with the detector one via a 6" CF flexible bellows.

93 The IV is made of 1.5" height cylinder with 6" CF flanges on the top and bottom parts of it,  
 94 and it holds inside xenon. A 120 mm diameter cold finger is welded to the top flange of the IV.  
 95 The design of the cold finger is similar to the design of [13], the inner part of the cold finger is  
 96 made of long fins, therefore the surface area of it is bigger resulting in a better heat transport. The  
 97 upper part of the cold finger is in thermal contact with the cryo-cooler<sup>1</sup> via a cooper adapter. The  
 98 copper adapter holds two 100Ω pt resistor which are connected to a PID reader<sup>2</sup> for temperature  
 99 measurements. A Cartridge-heater is also inserted to the copper adapter for emergency heating.

<sup>1</sup>QDrive 20BB 9p6 A 3 AYNBNCO

<sup>2</sup>cryo-con model 18i Cryogenic Temp Monitor

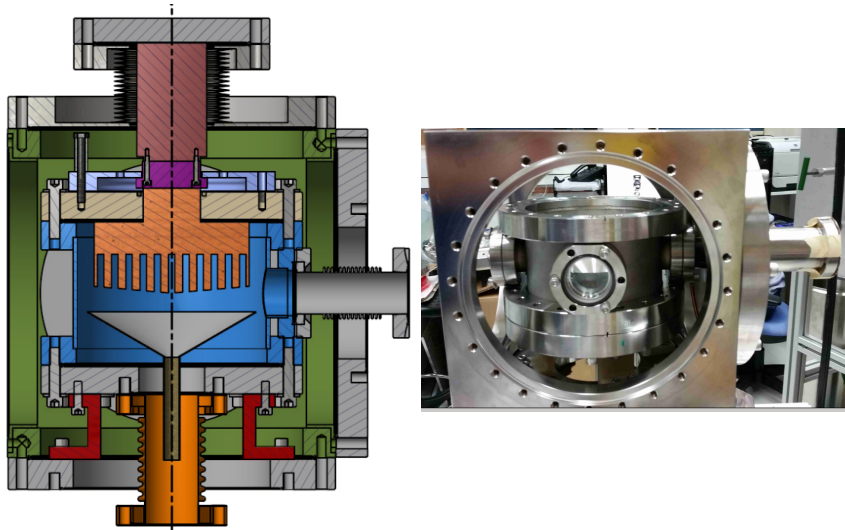


**Figure 3.** CAD view of the cryogenic system(Left) and a pictue of the cryogenic system (Right) .

100        The cryo-cooler provides up to 70 W of cooling power, and is connected via a  $4\frac{1}{2}$ " flange to  
 101      the OV top flange, and reaching the IV top flange. Common cryo-coolers used for xenon experi-  
 102      ments, work in maximal cooling mode permanently. The QDrive, instead, has temperature control  
 103      allowing it vary the cooling power, which enables to set the temperature with fluctuations smaller  
 104      then 0.1 C° on the cooler itself.

105        On the inner side of the bottom flange of the IV a thin SS funnel is installed collecting all LXe  
 106      drops from the cold finger, and delivering them to the detector part. This flange is connected to  
 107      the detector part, via a  $3\frac{3}{8}$ " flexible bellows. This bellows hosts two small pipes connected to the  
 108      circulation system, and a third pipe coming from the funnel, all three pipes deliver LXe whereas the  
 109      GXe is filling the bellows. The separation between the LXe coming from the gas handling system  
 110      (clean) and the LXe coming from the cold finger (more dirty) allows the filling of clean LXe to  
 111      different parts of the detector.

### 112      **2.3 The Detector**

113      [MMD: The detector refers to the chamber and its inner assembly that contains the liquid Xenon  
 114      bubble, the photomultiplier detectors around it and their accessories. This chamber is placed below  
 115      the cryogenic system. We describe the detector chamber and its interface to the cryogenic system  
 116      in section 2.3.1. In section 2.3.2 we discuss the assembly that consists of the HPFS sphere to hold  
 117      liquid Xenon and the Photomultiplier detectors distributed around the sphere.]

#### 118      **2.3.1 The Detector Chamber**

119      The detector chamber is built such that apart from the interface to the cryogenic system, it can be  
 120      changed and modified easily for future experiments. The interface unit is built out of 2 flanges  
 121      welded together via 7 tubes, which serve as service ports for electrical and other feedthroughs. The  
 122      upper flange, ISO-K NW320, is part of the OV and shares the insulation vacuum of the cryogenic  
 123      system, the bottom one , CF-8", is part of an IV for future detectors, and would hold xenon inside.  
 124      For our experiment we modified the CF flange to fit also a  $4\frac{5}{8}$ " CF flange which we use.

125        The OV is closed with a cylinder XXX cm height closed from the bottom with another ISO-K  
126        NW320 flange, the height of the cylinder is determined such that the maximal height of the whole  
127        apparatus is 190 cm, allowing the mobility of the detector through standard doors.

128        The  $4\frac{5}{8}$ " CF flange is connected to a closed vessel internally divided into two parts. This vessel  
129        serves as a xenon reservoir. The two parts of the vessel are connected to a spherical orb from above  
130        (inner part) and from below (outer part). LXe is circulated such that new LXe drips into the outer  
131        part and pumped from the inner one. This way the liquid level is controlled, and the sphere itself is  
132        always filled with LXe.

### 133        2.3.2 The Sphere

134        The central component of the detector assembly is the hollow sphere which holds the LXe target  
135        bubble. A spherical shell made of high purity fused silica with high transmittance is designed to  
136        hold the LXe target. The xenon will be circulated Two invar tubes are connected to it from the top  
137        and bottom with SS mini-CF flanges at the end, to circulate the xenon (see Fig.~??). The bottom  
138        flange of the sphere is held using a brass holder to prevent force or torque applied on the sphere  
139        while mounting the detector. The brass holder is connected to a plate held from the top 8" flange,  
140        and is also used to align this plate at first installation. A set of 20 PMTs<sup>1</sup> are placed around the  
141        sphere to detect light emitted from the LXe.

142        The LXe target bubble should not be too large in order to avoid double scatters. This shell  
143        should be large enough to reduce internal reflections, but not too large which would attenuate the  
144        scintillation light. The material of the shell should have a refractive index similar to LXe in order  
145        to have minimal diffraction from the original direction of the photons when they travel from the  
146        LXe target to the sphere. We chose corning HPFS 8655 as the shell material. The refractive index  
147        of HPFS 8655 is 1.575 at 185 nm (LXe R.I. 1.61). In Fig. 4, are the refractive indices at various  
148        wavelengths as given by the HPFS factsheet and also a naive extrapolation at lower wavelengths  
149        which are relevant to us.

150        The transmittance of the material is extremely crucial for us to optimize the dimension of the  
151        shell. Therefore, we obtained a 6 mm thick sample of HPFS 8655 and performed a transmittance  
152        testing a VUV monochromator setup. A deuterium light source was used to generate a spectrum  
153        in the range (110 - 950) nm, peaked approximately at 160 nm. The window of the light source  
154        faced a vacuum space pumped to below  $10^{-4}$  Torr. The monochromator allows to select the desired  
155        wavelengths using a manually rotatable holographic diffraction grating. A PMT placed in the  
156        vacuum measured the intensity of light emitted from the monochromator, with and without the  
157        fused silica sample. The ratio of measured intensities was used to calculate the transmittance of  
158        the material. In fig. 5 is the measured transmittances/ 6 mm at (150 - 215) nm. At 175 nm the  
159        sample shows approximately 90%/6mm measured transmittance which corresponds to an intrinsic  
160        transmittance of about 98%.

161        The dimension of the fused silica shell is optimized by studying the path of the scintillation  
162        photons using a GEANT4 based simulation [14]. The sources that will be used for exciting the  
163        xenon, and creating the superradiance (signal) as well as the standard emission (background), will  
164        be  $^{137}\text{Cs}$  (662 keV) and  $^{57}\text{Co}$ (122keV & 136 keV) for ER and  $^{241}\text{AmBe}$ , D-D neutron generator,

---

<sup>1</sup>r8520-406 Hamamatsu 1" PMT

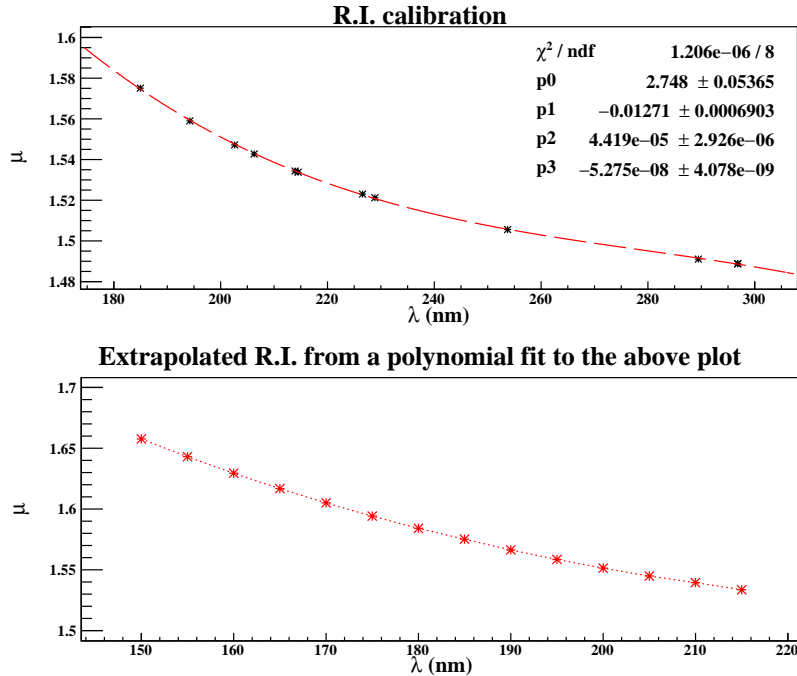


**Figure 4.** The refractive indices of HPFS 8655 at various wavelengths. (Top) The values provided from Corning factsheet. (Bottom) The values extrapolated at lower wavelengths.

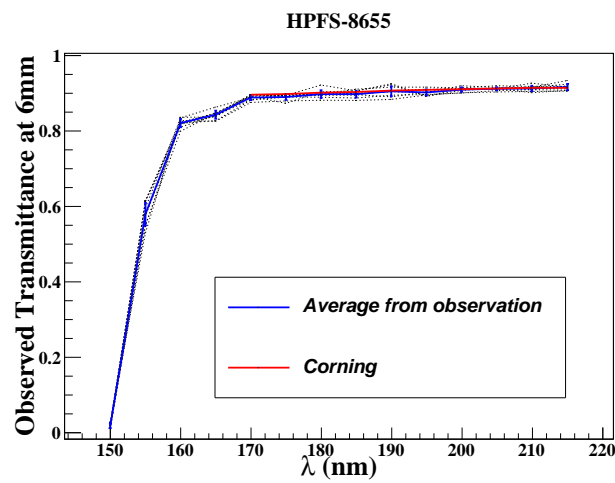


**Figure 5.** The transmittance of a 6 mm thick HPFS 8655 sample.

165 or neutron produced in an accelerator for NR . The mean free path for this energy is a couple of  
166 mm ( $^{57}\text{Co}$ ) and (0.5 - 3) cm ( $^{137}\text{Cs}$ ). We discuss the simulation in detail in section 4. The outer  
167 radius of the shell is 3 cm, while the inner radius of the hollow space that will hold the LXe is 1  
168 cm. The flow of the LXe will be maintained by two invar tubes. This shell–system, as is shown in  
169 Fig. ?? is being manufactured industrially as per the specification provided by us.

170 The photons coming out of the system will be detected by twenty 1" square Hamamatsu  
171 R8520-406 photomultiplier tubes with an active area of 20.5 mm  $\times$  20.5 mm each. We pick PMTs  
172 with a minimum quantum efficiency of 30% at 178 nm. For an applied voltage of 900 V the gain  
173 of these PMTs are  $2 \times 10^6$ . We use a positive voltage divider, also manufactured by Hamamatsu,  
174 to provide high voltage to the PMTs. These 20 PMTs are held with a special aluminum holder,  
175 coated with anti-reflection substance. The holder is made of two hemispheres hosting the PMTs  
176 in 3 rows all of them pointing to the center of the fused-silica sphere. the PMTs are held only  
177 via their voltage–divider bases. The bases are held using M2 PEEK screws. In Fig. 6, one of the  
178 holder–hemispheres with the PMTs are shown.

179 In Fig. 7 we present a CAD schematic as well as a real view of the detector part.

### 180 3 The Data Acquisition (DAQ) System

181 [MMD: This part is almost complete, trigger logic details might get changed slightly]

182 In this section we discuss the data acquisition and readout from the PMT channels. We use a  
183 heterogeneous system consisting of both NIM and VME electronics modules, with the data readout  
184 being carried out through the VME controller module V2718 and a PCIe card A3818.

185 The schematic layout of the DAQ system is shown in Fig. 8. All the 20 PMTs are oriented  
186 in the holder assembly which was discussed in section 2.3.2. The PMTs are ramped up to +800V  
187 (the maximum is +900V) using a 24 channel VME high volatge distributor module <sup>1</sup>. We define  
188 the raw electrical pulse output of the PMTs as  $S_i$  (raw), where  $i = 1 - 20$ . These raw pulses are  
189 then amplified and shaped using two photomultiplier preamplifiers <sup>1</sup>. The preamplifier channels  
190 operates from DC to 275 MHz and produce two identical  $50 \Omega$  non inverting outputs with voltage  
191 gains of 10. We define the amplified pulses as  $S_i$ , ( $i = 1 - 20$ ). One out of the two identical analog  
192 outputs from each channel is converted to a digital signal with an Analog to Digitizer converter <sup>2</sup>.

193 The ADC consists of two 12bit 5GS/s Switched capacitor Digitizer sections, each of them  
194 with 16+1 channels, based on DRS4 chip. The dynamic range of the input signal is 1 Vpp with  
195 adjustable DC offset. This module can sample either bipolar or unipolar analog input signal within  
196 the dynamic range in a circular analog memory buffer, with default sampling frequency choices  
197 5GS/s, 2.5 GS/s or 2 GS/s. As soon as a trigger signal reaches, all the analog memory buffers gets  
198 frozen and then gets digitized into a digital memory buffer with a 12 bit resolution.

199 We generate an intrinsic trigger for the system, with the coincidence of any two out of the  
200 twenty PMTs. The second output from the preamplifier channels are converted to binary signals  
201 using two 16 channel leading Edge discriminator <sup>3</sup>. In Fig. 8, we term the binary outputs from the

---

<sup>1</sup>iseg VDS18130p

<sup>1</sup>Phillips 776. Each of the preamplifier model provides 16 independent and direct-coupled amplifiers channels

<sup>2</sup>CAEN ADC V1742: Switched capacitor Digitizer

<sup>3</sup>CAEN V895



**Figure 6.** The technical scheme of the HPFS shell with invar tubing and flanges.

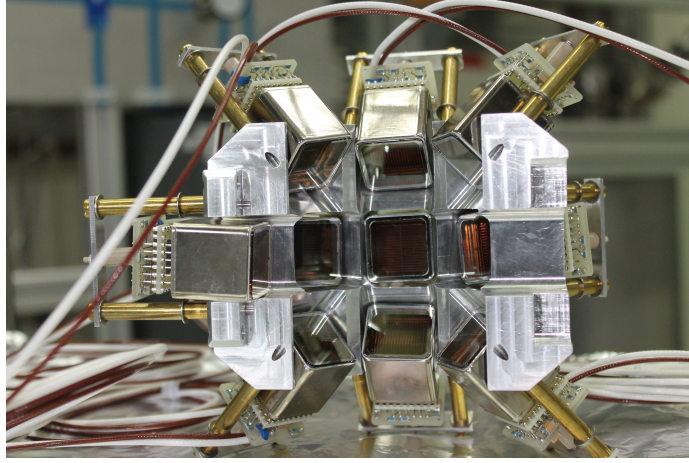


**Figure 7.** A PMT holder–hemisphere. We use two such components to hold 20 PMTs around the target.

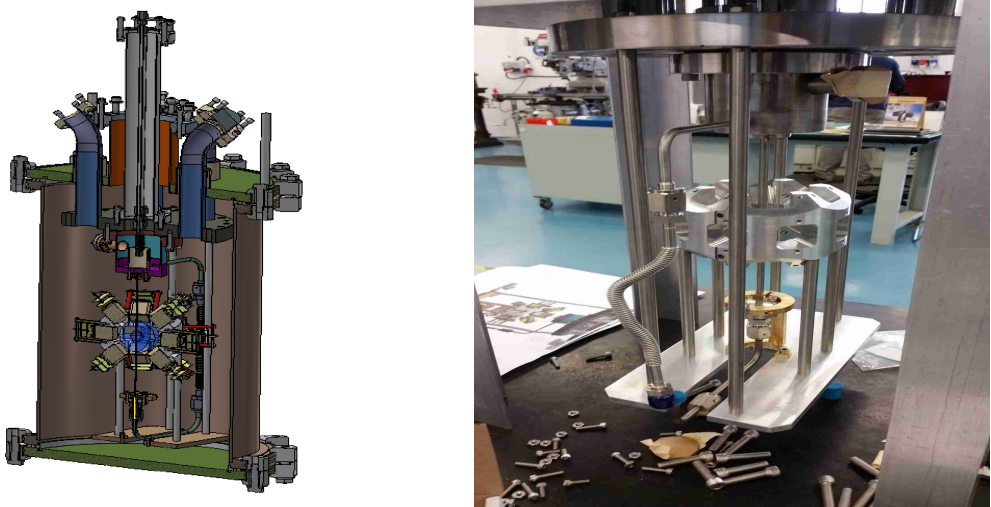


**Figure 8.** (Left) CAD design of the detector part. (Right) First mounting of the detector part, still not connected to the rest of the system.

discriminator as SD $i$ ,  $i = 1 - 20$ . The SD $i$  signals are then passed over to the logic module <sup>4</sup> to obtain the trigger. At present, the coincidence of any two out of the twenty PMTs forms the trigger logic. The output of the logic operation is used to trigger the ADC. In order to record the PMT noise rate, the SD $i$  signals are duplicated and fed to a scaler <sup>5</sup>.

The PMT event information and the trigger rate are read from the ADC, while the Scaler records the PMT noise rate. The data readout to the acquisition PC is done through the Controller and optical link to the master PCIe card. The further analyses of the relevant events in the PMTs will be carried out offline using an analysis framework.

---

<sup>4</sup>CAEN V1495, an FPGA based General purpose VME board which is programmed to perform the logic operation

<sup>5</sup>CAEN V830

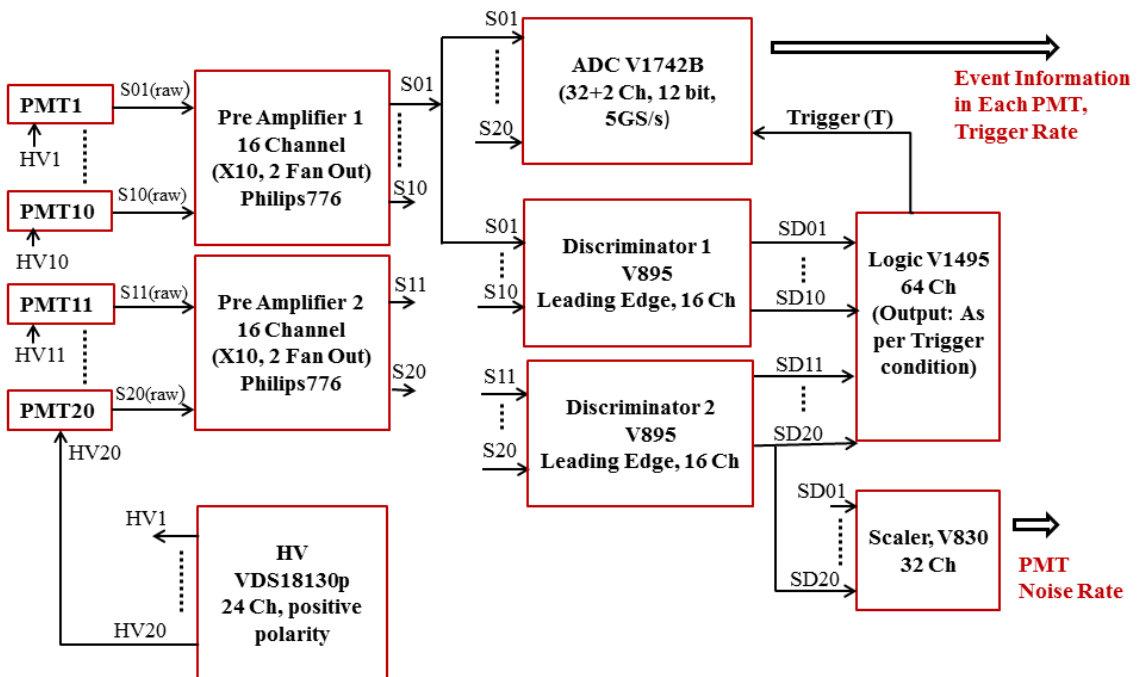


**Figure 9.** The schematic of the Data Acquisition System of Direxeno. It consists of 20 PMTs and the subsequent electronic channels to record the events for an internal trigger generated by the coincidence of any two PMTs in the system and also the PMT noise rate.

210 **4 Simulation**

211 In this section we present the Monte Carlo simulation study that was performed to optimize the  
212 geometry and performance of the LXe scintillation detection system. We perform a GEANT4 based  
213 simulation to obtain the reasonable dimensions of the spherical LXe holder and the placement of the  
214 PMT detectors around it, which is described in section 4.1. In section 4.2, we discuss the statistical  
215 test performed to find the detector’s sensitivity in measuring various patterns of the scintillation  
216 emission from the LXe target.

217 **4.1 The Detector Geometry**

218 We perform a study to optimize the dimensions of the setup using a GEANT4 based framework  
219 that includes realistic description of the target, the enclosing HPFS sphere and the PMTs around.  
220 The simulations takes into account the physics processes of the propagation of the photons from  
221 the LXe target through the the sphere and the vacuum and their interaction at the PMTs. The  
222 parameters under test for this study are the size of the sphere, the PMT size and their placement  
223 around the sphere. The refractive index and internal transmittance of both of LXe and of HPFS are  
224 known with good precision.

225 For the simulation, we fix all parameters except the outer radius ( $R_2$ ) of the sphere. The fixed  
226 parameter values are chosen by quantitative physical considerations and educated guesses. The  
227 radius of the LXe target  $R_1$  will determine the event rate for a particular source, and we choose  
228 it to be 1 cm. The conventional PMTs designed by Hamamatsu to detect scintillation from LXe  
229 are 1" and 3" square PMTs, and we choose the 1' ones in order to get better spatial resolution. an  
230 array of 20 PMTs around the sphere, placed at a distance of 39 mm from the centre of the targetare  
231 considered. The active area of each PMT is 22 mm  $\times$  22 mm.

232 In order to chose a reasonable dimension of the sphere, we first study the detection efficiency  
233 of scintillated photons in the simulated setup. Using an inotropic emmision of 50photons/event,  
234 we find the average ratio of the detected photons/event to the net emitted photons/event, for various  
235 choices of  $R_2$ . The trasmittance of HPFS is a crucial parameter and we vary it within a large range  
236 to check the impact of it. The photon detection ratio for different sets of  $R_2$  and transmittance are  
237 shown in Fig. ??.

238 **4.2 The statistical test**

239 **5 Summary**

240 **References**

- 241 [1] E. Aprile and T. Doke. Liquid Xenon Detectors for Particle Physics and Astrophysics. *Rev. Mod.*  
242 *Phys.*, 82:2053–2097, 2010.
- 243 [2] A. Rubbia. Future liquid Argon detectors. 2013. [*Nucl. Phys. Proc. Suppl.* 235-236, 190(2013)].
- 244 [3] J. Silk et al. *Particle Dark Matter: Observations, Models and Searches*. Cambridge Univ. Press,  
245 Cambridge, 2010.
- 246 [4] E. Aprile et al. First Dark Matter Search Results from the XENON1T Experiment. 2017.

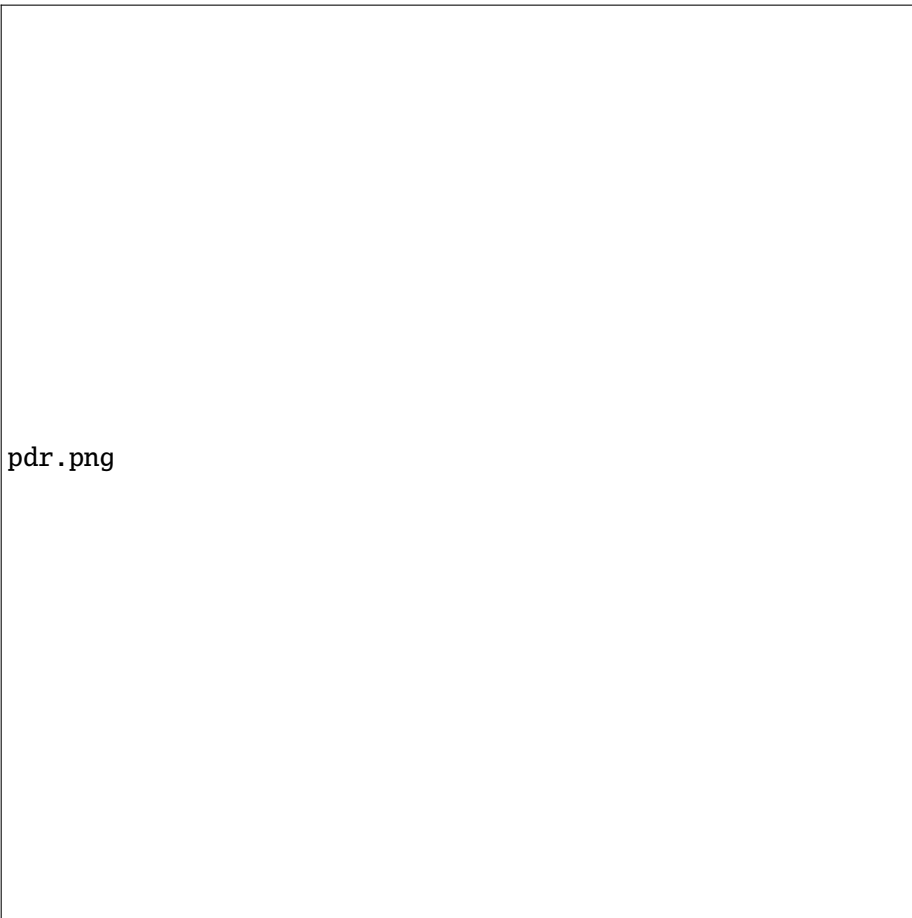


**Figure 10.** The photon detection ratio as a function of  $R_2$ , for different transmittances of the fused silica shell. We use  $10^4$  events with 50 photons/event for each choice of transmittance and  $R_2$

- 247 [5] D. S. Akerib et al. Results from a search for dark matter in the complete LUX exposure. *Phys. Rev.*  
248 *Lett.*, 118(2):021303, 2017.
- 249 [6] Changbo Fu et al. Spin-Dependent Weakly-Interacting-Massive-ParticleâŠNucleon Cross Section  
250 Limits from First Data of PandaX-II Experiment. *Phys. Rev. Lett.*, 118(7):071301, 2017.
- 251 [7] J. Aalbers et al. DARWIN: towards the ultimate dark matter detector. *JCAP*, 1611:017, 2016.
- 252 [8] R. H. Dicke. Coherence in spontaneous radiation processes. *Phys. Rev.*, 93:99–110, Jan 1954.
- 253 [9] M. Gross and S. Haroche. Superradiance: An essay on the theory of collective spontaneous emission.  
254 *Physics Reports*, 93(5):301 – 396, 1982.
- 255 [10] N G Basov, V A Danilychev, and Yurii M Popov. Stimulated emission in the vacuum ultraviolet  
256 region. *Soviet Journal of Quantum Electronics*, 1(1):18, 1971.
- 257 [11] Frederick H. Mies. Stimulated emission and population inversion in diatomic bound-continuum  
258 transitions. *Molecular Physics*, 26(5):1233–1246, 1973.
- 259 [12] K L Giboni, X Ji, H Lin, A Tan, T Ye, Y Zhang, and L Zhao. A liquid xenon development and test  
260 system. *Journal of Instrumentation*, 9(04):T04006, 2014.

- <sup>261</sup> [13] E. Aprile et al. The XENON100 Dark Matter Experiment. *Astropart. Phys.*, 35:573–590, 2012.
- <sup>262</sup> [14] S. Agostinelli et al. GEANT4: A Simulation toolkit. *Nucl. Instrum. Meth.*, A506:250–303, 2003.